Solar Phys (2008) 253:
DOI 10.1007/s11207-008-9275-8

Peak Frequency Dynamics in Solar Microwave Bursts

V. F. Melnikov[1,2] · **Dale E. Gary**[1] · **Gelu M. Nita**[1]

Received: 21 March 2008 / Accepted: 21 September 2008 / Published online: 16 October 2008

Abstract We analyze the dynamics of the broadband frequency spectrum of 338 microwave bursts observed in the years 2001–2002 with the Owens Valley Solar Array. A subset of 38 strong microwave bursts that show a single spectral maximum are studied in detail. Our main goal is to study changes in spectral peak frequency $\nu_{\rm pk}$ with time. We show that, for a majority of these simple bursts, the peak frequency shows a high positive correlation with flux density—it increases on the rise phase in $\approx 83\%$ of 24 bursts where it could be cleanly measured, and decreases immediately after the peak time in $\approx 62\%$ of 34 bursts. This behavior is in qualitative agreement with theoretical expectations based on gyrosynchrotron self-absorption. However, for a significant number of events ($\approx$ 30-36%) the peak frequency variation is much smaller than expected from self-absorption, or may be entirely absent. The observed temporal behavior of $\nu_{\rm pk}$ is compared with a simple model of gyrosynchrotron radio emission. We show that the anomalous behavior is well accounted for by the effects of Razin suppression, and further show how an analysis of the temporal evolution of $\nu_{\rm pk}$ can be used to uniquely determine the relative importance of self-absorption and Razin suppression in a given burst. The analysis technique provides a new, quantitative diagnostic for the gyrosynchrotron component of solar microwave bursts. Applying this analysis technique to our sample of bursts, we find that in most of the bursts (60%) the spectral dynamics of $\nu_{\rm pk}$ around the time of peak flux density is caused by self-absorption. On the other hand, for a significant number of events ($\approx$ 70%), the Razin effect may play the dominant role in defining the spectral peak and dynamics of $\nu_{\rm pk}$, especially on the early rise phase and late decay phase of the bursts.

Keywords: Flares, Dynamics; Radio Bursts, Dynamic Spectrum; Radio Bursts, Microwave

1. Introduction

Microwave broadband emission during solar flares can give us valuable information about processes of particle acceleration and transport, as well as about magnetic

[1] Physics Department, NJIT, University Heights, Newark, NJ, 07102, USA email: dgary@njit.edu email: gnita@njit.edu
[2] Radiophysical Research Institute (NIRFI), Nizhny Novgorod, 603950, Russia email: melnikov@nirfi.sci-nnov.ru

field and plasma density in solar flaring loops (see for review Bastian, Benz, and Gary, 1998; Fleishman and Melnikov, 2003; Lee, 2004; Bastian, 2006).

Studies of the shape of observed solar microwave spectra started in the early 1960s (Takakura and Kai, 1961; Takakura and Kai, 1966). A detailed analysis of the shape of microwave flux density spectra was done by Guidice and Castelli (1975). Their analysis was based on data obtained at fixed, well-separated frequencies. Theoretical studies, motivated by the observational findings, showed that the solar broadband microwave bursts are generated by nonthermal electrons via the gyrosynchrotron (hereafter GS) emission mechanism (Takakura and Kai, 1966; Ramaty, 1969; Takakura, 1972; Petrosian, 1981) and provided some simplified schemes for microwave diagnostics of solar flares (Dulk and Marsh, 1982; Gary, 1985; Klein,, 1987).

The spectrum of such emission usually has a characteristic shape, with a single peak at the peak frequency $\nu_{\rm pk}$. Emission above $\nu_{\rm pk}$ falls because the emission is optically thin, with the spectral slope being determined chiefly by the electron energy distribution, while $\nu_{\rm pk}$ and the low frequency slope may be determined either by self-absorption (Twiss, 1954) or by Razin suppression (Razin, 1960a). Different parts of the microwave burst spectrum give different tools for flaring loop diagnostics. For example, the high frequency slope, flux density, and polarization of emission at $\nu > \nu_{\rm pk}$ can provide information about the spectral index of nonthermal electrons (Klein, Trottet, and Magun, 1986), total number of high energy electrons, and also about pitch-angle anisotropy (Fleishman and Melnikov, 2003). The low frequency slope and flux density strongly depend on magnetic field strength and inhomogeneity and on effective energy of emitting electrons. They also may depend on the ratio of plasma density and magnetic field if Razin suppression is important.

One of the key parameters of a solar microwave burst is the frequency $\nu_{\rm pk}$ of spectral maximum. Together with the peak flux, $S_{\rm pk}$, it gives information about magnetic field strength and column number density of nonthermal electrons (Gary and Hurford, 2004). In the case of strong Razin suppression these parameters can also provide information about volume density in a flaring loop. Certain high-density flares, which necessarily have strong Razin suppression, may also show $\nu_{\rm pk}$ evolution due to changes in free-free absorption as plasma heating takes place, as in the event discussed in detail by Bastian, Fleishman, and Gary (2007).

Striking results were obtained in the comprehensive, multi-frequency study by Stähli, Gary, and Hurford (1989). They studied 49 bursts and found that for majority of the bursts the deviation of $\nu_{\rm pk}$ during the rise and decay phases of bursts was much less than that predicted by the theory of GS radiation (Dulk and Marsh, 1982). Using the simplified expressions for GS emission from a homogeneous radio source (Dulk and Marsh, 1982), they analyzed how the peak frequency was affected by such parameters as 1) magnetic field strength B, 2) column number density of nonthermal electrons along line of sight nL, 3) the viewing angle θ with respect to magnetic field direction, and 4) the size of a radio source Ω. They pointed out that a change in the burst source size has no effect on the peak frequency, but that an increase in any other source parameter results in an increase in the peak frequency. As an explanation of the constancy of $\nu_{\rm pk}$ during a burst, the authors suggested that for most of the events the source parameters (number of energetic electrons and/or magnetic field strength) may vary over the course of a burst in such a way that the peak frequency does not change.

A comprehensive analysis of the peak frequency evolution for one particular flare was done by Belkora (1997). In her analysis she used OVSA observations with spatial resolution, so it was possible to derive the brightness temperature spectrum rather than the total flux density spectrum. A striking peculiarity of the burst was that the peak frequency remained nearly constant while the peak brightness temperature varied over two orders of magnitude. As an explanation, Belkora suggested the Razin effect. If Razin suppression is present, only a change in the number of nonthermal electrons is required to cause the observed change in brightness temperature. The steep low frequency slope of the observed burst spectrum gave additional support for Razin suppression. The parameters required to explain the event in terms of the Razin effect are electron density $n_{\rm e} = 2 \times 10^{11}$ cm^{-3} and magnetic field $B = 300$ G, respectively.

The main purposes of our present study are to: a) show that the wide range of behavior in peak frequency evolution seen in our large sample of bursts can be explained in terms of two competing effects, self-absorption and Razin suppression, b) develop an analysis procedure to distinguish between the two effects using the temporal behavior of the microwave spectrum, c) investigate statistically which effect is dominant at which times during a typical burst evolution, and d) determine in what percentage of bursts each effect is important. To accomplish this, we conduct a statistical study of 338 microwave bursts obtained during the period 2001–2002 with the Owens Valley Solar Array (Nita, Gary, and Lee, 2004). For 38 events selected for their relatively simple time profiles, we perform a detailed analysis of the spectral evolution of $\nu_{\rm pk}$.

In Section 2 we present observations and in Section 3 the results of data analysis. We find that the bursts divide naturally into a few distinct types with specific temporal behaviors during their rise and decay. In Section 4 we carry out simple numerical modeling of each type to show that the types correspond to differences in the relative importance of GS self-absorption and Razin suppression. In the last section we compare empirical and calculated features of the spectral evolution and summarize our results.

2. Observational Data

The data for this study come from the set of events analyzed by Nita, Gary, and Lee (2004), namely 412 bursts observed in microwaves with the solar-dedicated Owens Valley Solar Array (OVSA). After some upgrades (Gary and Hurford, 2000) the array operated during this study with six antennas (two 27 m dishes and four 2 m dishes). OVSA data comprise both total power from each antenna and correlated amplitudes and phases from each baseline (pair of antennas), but this study is limited to total power (integrated flux density, without spatial resolution). Because of difficulties with absolute flux calibration of the 27-m dishes due to their restricted field of view, we further limit our analysis to data from the 2-m antennas, and hence discuss only total intensity (Stokes I). The 2-m dishes have a total power sensitivity of a few solar flux units (sfu; 1 sfu = 10^{-22} W m^{-2} Hz^{-1}). The data are taken at typically 40 frequencies, distributed approximately logarithmically from 1 to 18 GHz, with 4 s time resolution. The 2-m flux calibration is based on the quiet Sun total flux density as reported by the National Oceanic and Atmospheric Administration (NOAA). See Nita, Gary, and Lee (2004) for

details of the calibration procedure. OVSA data are highly suitable for studies of the peak frequency evolution of GS spectra due to OVSA's relatively large number of closely spaced frequencies covering the relevant range of 1–18 GHz over which most bursts have their spectral maximum.

The 412 bursts analyzed by Nita, Gary, and Lee (2004) included decimetric bursts with no clear GS component. For this study we restrict our initial selection to bursts with well defined spectral peaks in the range $\nu_{\rm pk} = 3 - -16$ GHz, which are identified with GS emission. This results in a total of 338 events used in this study.

After calibration, we performed a 4-parameter fit to the burst spectrum at each time using the generic function introduced by Stähli, Gary, and Hurford (1989):

$$S(\nu) = a_1\ \nu^{\ a_2}\ [1 - \exp(-a_3\ \nu^{-a_4})], \tag{1}$$

which yields four physically relevant parameters, the low frequency spectral index (a_2), the high frequency spectral index ($\alpha_{\rm h} = a_4 - a_2$), the peak, or turn over frequency ($\nu_{\rm pk}$) and the peak flux $S(\nu_{\rm pk})$. This generic function has a shape similar to the GS emission spectrum obtained using the simplified formulas by Dulk and Marsh (1982). An example of such fitting is shown in Figure 1. In some events the low frequency part of the spectrum contains an additional low frequency spectral peak, $\nu_{\rm pk} \approx$ 1–2 GHz (Nita, Gary, and Lee, 2004; Fleishman, Nita, and Gary, 2005). In these cases we limit the range of frequencies by a reasonable value $\nu_{\rm min}$ that varies from burst to burst, but was generally around 2–3 GHz.

In addition to our statistical study of the 338 bursts, we also performed a more detailed analysis of a much smaller subset of bursts. To avoid complexities due to overlapping spectral or temporal components, for the detailed study we selected only bursts having a single, well defined spectral peak at the burst maximum and a simple time profile with peak flux density $S_{\rm pk} > 100$ sfu. This selection reduced the 338 bursts to a total of 40 events. We checked the flare locations for these 40 events from the NOAA Geophysical Data Center and found that two events in 2001 December were located at the limb and may have been partially occulted. We have dropped these from further consideration, leaving 38 bursts for more in-depth study.

3. Peak Frequency Dynamics

Comparison of spectra at different times during a burst clearly shows a change of peak frequency with time for most of the bursts in our data set. In Figure 1 we show an example of the typical spectral evolution. In this figure, spectra at different times are plotted in two panels, separately for the rise phase and decay phase. We can see a considerable increase of $\nu_{\rm pk}$ on the rise phase and then a decrease after the burst maximum. A remarkable feature of the spectral evolution in this example is the much faster increase of the flux at frequencies $\nu > \nu_{\rm pk}$ than at $\nu < \nu_{\rm pk}$, which is an indication that the source is optically thick at $\nu < \nu_{\rm pk}$. In what follows, we use a parameter, R, that serves as a measure of the difference in rate of change of flux density on either side of the spectral peak. We define it as:

$$R = \log \frac{S(\nu_2)}{S(\nu_1)}, \tag{2}$$

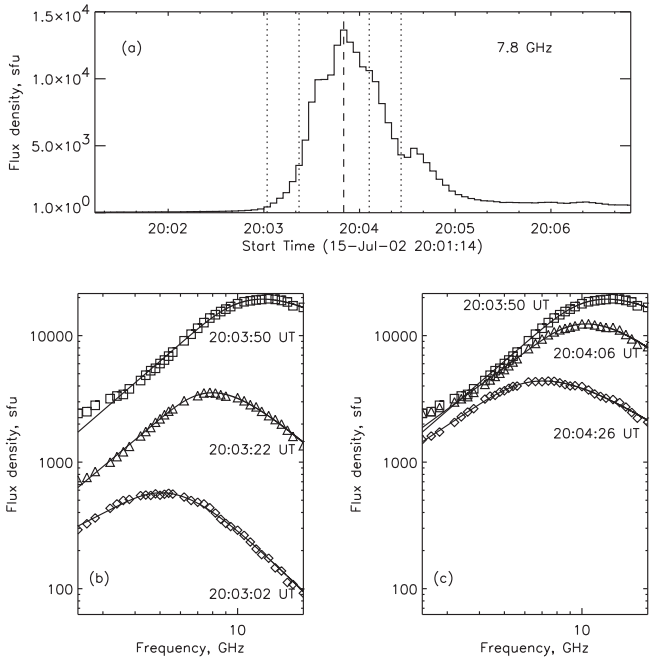

Figure 1. Spectral evolution of the first peak in the microwave multi-component burst of 15 July 2002. Solid lines show the best fit with the generic function Equation (1). An increase of the turnover frequency on the rising phase (left panel) and a corresponding decrease on the decay phase (right panel) is clearly seen.

where $\nu_1 < \nu_{\rm pk}$ and $\nu_2 > \nu_{\rm pk}$ are frequencies (constant for a given burst) that are well away from $\nu_{\rm pk}$. For definiteness, we define $\nu_1 = (\nu_{\rm pabs} + \nu_{\rm min})/2$, $\nu_2 = (\nu_{\rm pabs} + \nu_{\rm max})/2$, where $\nu_{\rm pabs}$ is the absolute maximum of $\nu_{\rm pk}(t)$ during a burst, and $\nu_{\rm min}$, $\nu_{\rm max}$ indicate the frequency range in which the burst was detected. It is not the value of R that is of interest, but only its behavior with time. As we show quantitatively in Section 4, a ratio R that increases during the rise phase and decreases during the decay indicates that the spectral turnover is due to self-absorption, while a relatively constant R indicates that frequencies on both sides of the turnover frequency are optically thin—a signature of Razin suppression. In contrast to the burst in Figure 1, the burst in Figure 2 displays constant R throughout the rise and most of the decay. This is an excellent example of a burst for which Razin suppression would be suspected, as further indicated by the constancy of the peak frequency over most of the burst.[1]

Time profiles for several key spectral parameters of the event shown in Figure 1 are represented in Figure 3. The three parameters $S_{\rm pk}$ (panel (a)), $\nu_{\rm pk}$ (panel

[1]A traditional spectral signature of Razin suppression, a steep low-frequency slope (Klein, 1987), is not seen in this burst, and in fact is rare in spatially integrated total power spectra. In the Appendix we show that plasma density inhomogeneity, expected for flaring loops, can flatten the low frequency GS spectrum even in the presence of significant Razin suppression in the main part of a radio source. Additional flattening can occur due to magnetic field inhomogeneity (*e.g.* Preka-Papadema and Alissandrakis, 1988).

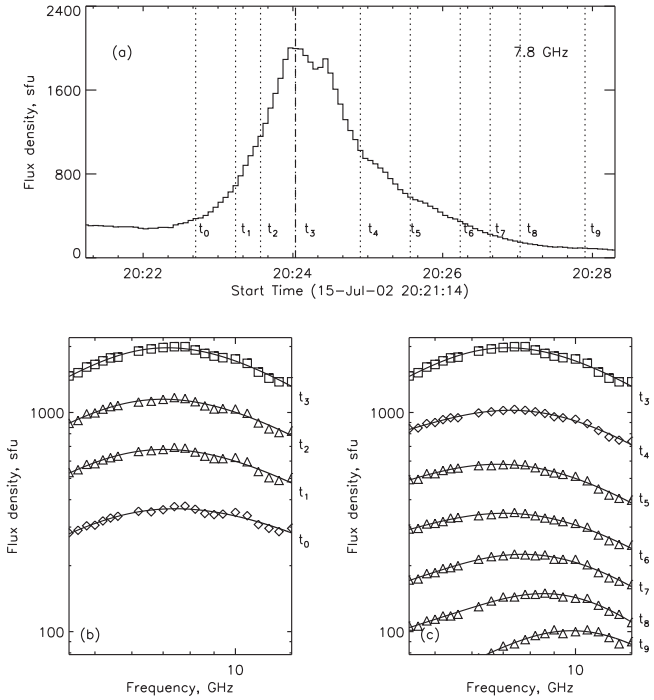

Figure 2. Spectral evolution as in Figure 1 for a secondary peak in the microwave burst of 15 July 2002. Note the remarkable stability of the peak frequency during the most of the burst, the equal rise and fall on both sides of the peak frequency (which yields a constant R, and as well as its increase and steepening of the spectra at low frequencies on the late decay phase.

(b)), and R (panel (c)) all show a clear, positive correlation. The high-frequency spectral index $\alpha_{\rm h}$ in panel (d) shows a low positive correlation in this burst. It is an important parameter, however, as it gives a measure of the evolution of the nonthermal electron energy distribution.

To determine how common is the correlation shown in Figure 3(a) and (b), we plot in Figure 4 the distribution of correlation coefficients between $\nu_{\rm pk}$ and $S_{\rm pk}$ separately for the rise and decay phases for those bursts from our dataset that had sufficiently clean rise and decay phases (at least in the time interval where the flux is over 70% of maximum). The number of bursts used in Figure 4(a) is 202, and the number used in Figure 4(b) is 216.

It is clearly seen from the distributions that there is a large subset of bursts with strong positive correlation (correlation coefficient $r > 0.5$) between peak frequency and peak flux of a burst, both on the rise phase (50%) and on the decay phase (52%). However, a similar number of bursts show a random scatter of correlations, and a minor peak in the distribution occurs near $r = -1.0$, showing a distinct anti-correlation. We discuss anti-correlations further in Section 3.3.

Qualitatively, a positive correlation between the peak frequency and the burst flux is expected in the simple GS model, in which the low-frequency turnover occurs due to self-absorption. We can show this semi-quantitatively using the simplified formulas of Dulk and Marsh (1982). For the simple case of a homogeneous radio source, the emitted spectral flux density $S(\nu)$ is given by the radiation transfer

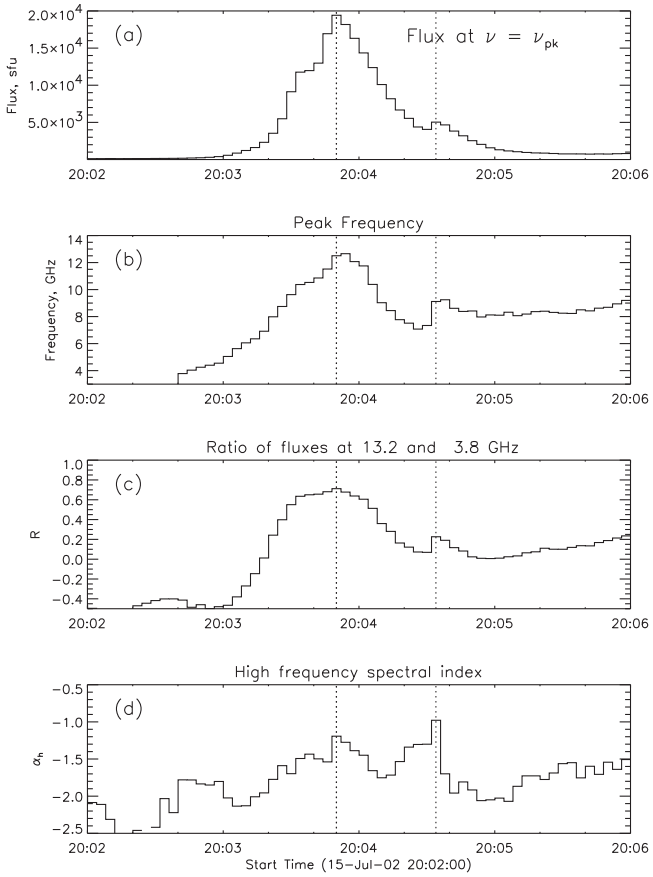

Figure 3. Time profiles of several key parameters of the spectral evolution of the burst shown in Figure 1: (a) Flux density, (b) peak frequency, (c) ratio R of fluxes at two frequencies, one (13.2 GHz) on the high-frequency side and one (3.8 GHz) on the low-frequency side of $\nu_{\rm pk}$, and (d) the high frequency spectral index, $\alpha_{\rm h}$. A strong correlation is seen among the top three panels, both on the rise phase and initial part of the decay phase. The dotted vertical lines in each panel mark the peak times in panel (a).

equation in the form:

$$S(\nu) = \frac{2k_{\rm B}T_{\rm eff}(\nu)}{c^2}\nu^2[1 - e^{-\tau(\nu)}] \times \frac{A}{R_{\rm s}^2}, \tag{3}$$

where $k_{\rm B}$ and c are the Boltzmann constant and velocity of light, $R_{\rm s}$ is the distance from the Sun to the Earth, and A is the area of the source. In general (Ramaty, 1969; Fleishman and Melnikov, 2003), the effective brightness temperature, $T_{\rm eff}(\nu)$, and optical thickness, $\tau(\nu)$, are complicated functions of the electron energy and pitch-angle distributions, magnetic field strength, B, viewing angle between the directions of magnetic field and the line of sight, θ, plasma density, n_0, and the source depth, L.

The flux density $S(\nu)$ reaches its maximum value, $S_{\rm pk}$, at the frequency $\nu = \nu_{\rm pk}$ where $\tau(\nu_{\rm pk}) \simeq 1$, so the expression $1 - e^{-\tau(\nu_{\rm pk})} \simeq 0.6$. In the case where the Dulk

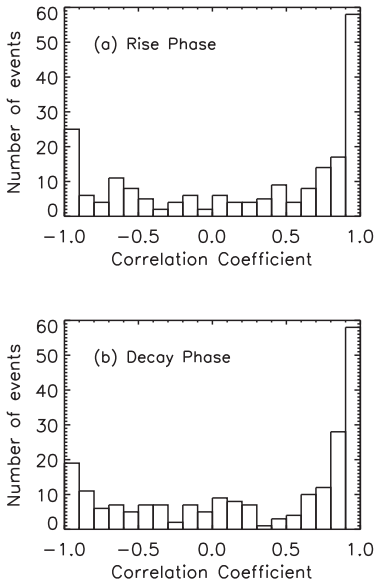

Figure 4. Distribution of correlation coefficients between the peak frequency $\nu_{\rm pk}$ and peak flux $S_{\rm pk}$ on the rise (upper panel) and decay (lower panel) phases of the bursts from our set of events.

and Marsh (1982) formulas are valid, *i.e.* for low plasma density and energetic electrons with an isotropic, single powerlaw energy distribution of spectral index δ, we obtain

$$S_{\rm pk} \simeq 1.9 \times 10^{-54.0-0.31\delta} (\sin\theta)^{-0.36-0.06\delta} \nu_B^{-0.50-0.085\delta} \nu_{\rm pk}^{2.50+0.085\delta}\ A, \quad (4)$$

where ν_B is the gyrofrequency. A positive correlation between the peak flux and peak frequency is clearly seen from Equation 4. Dulk and Marsh (1982) also give an expression for the peak frequency in this homogeneous model,

$$\nu_{\rm pk} \simeq 2.72 \times 10^{3+0.27\delta} (\sin\theta)^{0.41+0.03\delta} B^{0.68+0.03\delta} (nL)^{0.32-0.03\delta}, \quad (5)$$

which depends on the number density, n, of nonthermal electrons with energies $E > 10$ keV, their spectral index, magnetic field strength, viewing angle and the source depth, L. Note that $\nu_{\rm pk}$ does not depend on the source area A. As is seen from Equations (4) and (5), any increase or decrease of the electron column number density, nL, leads to a simultaneous increase or decrease of both the microwave flux density and the peak frequency (*cf.* Figure 8 of Bastian, Fleishman, and Gary, 2007).

The optically thin flux density is $S_{\rm thin} \propto$ emissivity $\times$ volume, and the optically thick flux density is $S_{\rm thick} \propto T_{\rm eff} \nu^2 A$. Using the GS formulas for emissivity and $T_{\rm eff}$ given by Dulk and Marsh (1982), we obtain the ratio

$$\frac{S_{\rm thin}}{S_{\rm thick}} \simeq 10^{4-0.21\delta} (\sin\theta)^{0.71\delta-0.07} \nu_1^{-2} \left(\frac{\nu_2}{\nu_B}\right)^{1.22-0.90\delta} B \left(\frac{\nu_1}{\nu_B}\right)^{-0.985\delta-0.72} (nL). \quad (6)$$

Thus, for GS emission, the ratio of these fluxes (and hence, $R = \log \frac{S_{\rm thin}}{S_{\rm thick}}$) should change in proportion to nL, B, and δ in a similar way as $\nu_{\rm pk}$ (Equation (5)) and $S_{\rm pk}$ (Equation (4)) do. Note that Equation 6 is valid only for a homogeneous source. In the real flaring loop the source is inhomogeneous and emission at different frequencies comes from different parts of the loop. So we should use different values of B, A and, possibly, δ for $S_{\rm thin}$ and $S_{\rm thick}$, but the general correlation of R with $S_{\rm pk}$ should remain.

We have checked the relationship between R and $\nu_{\rm pk}$ for all 38 events from our sample and found a strong correlation ($r > 0.5$), for 76% of events in the rise phase and for 70% of events in the decay phase. Only for 13% of events on the rising phase and 17% on the decay phase does the correlation between R and $\nu_{\rm pk}$ become negative.

However, in general, bursts show many different time behaviors and extent of $\nu_{\rm pk}$ variation during a burst. We can see in Figure 4 that there is a small but non-negligible percentage of bursts showing strong ($r < -0.5$) negative correlation (27% and 22% of all bursts for the rising and decay phases, respectively), as well as very poor or no correlation, $|r| < 0.5$ (23% and 26% of bursts). The same is true for the correlation between R and $S_{\rm pk}$. These spectral behaviors cannot be explained on the basis of GS self-absorption alone.

3.1. Magnitude of Peak Frequency Variations

For more careful analysis of the spectral evolution during the rise and decay phases, we selected only bursts with relatively simple time profiles and well defined peaks. The total number of such bursts is 38, including 24 with the smooth rise phase and 34 with the smooth decay phase.

To understand what follows, it is important to realize that solar flares are not symmetric about their peak time. During their rise phase, the changes are typically rapid and monotonic, resulting in relatively simple behavior in the key parameters. Their decay, in contrast, is often slower and may show confounding behaviors as the complex, energized system of magnetic fields and plasma adjust to its new configuration. A smooth decay in flux density may mask complex, non-monotonic evolution of plasma parameters, and indeed the disparity in numbers above—24 events with a smooth rise, and 34 events with a smooth decay—suggests this. This general trend is readily seen in the microwave peak frequency evolution we now discuss. The rise phase in our sample shows just a few, rather easily understood behaviors, while the decay phase is far more complex.

A simple measure of peak frequency variations is the overall shift in peak frequency during the burst. We show this shift in Figure 5, normalized by $\nu_{\rm pk}$, since we might expect larger shifts for larger $\nu_{\rm pk}$. Figure 5(a) shows the distribution of $\Delta\nu_{\rm pk}/\nu_{\rm pk}$ during the time over which the flux density increases from 25% to 100% of its maximum value, while Figure 5(b) shows the same during the decay to 25% of maximum. Almost all of the events (83%) on the rise phase have positive values of $\Delta\nu_{\rm pk}$, and most events (62%) on the decay phase have negative $\Delta\nu_{\rm pk}$ as expected for GS self-absorption. An interesting feature of the distributions is the relatively high percentage of events with small frequency shifts ($-0.1 < \Delta\nu_{\rm pk}/\nu_{\rm pk} < 0.1$): 33% and 30% for the rising and decay phases respectively. Note, however, that this is still a much smaller percentage than found by Stähli, Gary, and Hurford (1989). Another interesting feature is the high percentage of events (38%) with

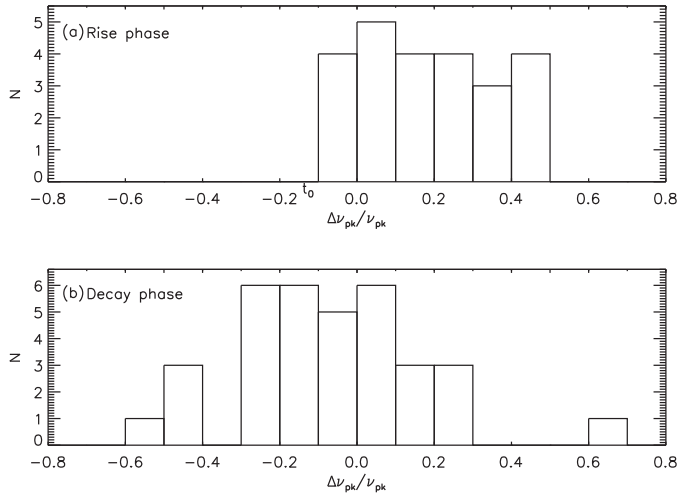

Figure 5. The distributions of shift in peak frequency, $\Delta\nu_{\rm pk}/\nu_{\rm pk}$, (a) on the rise and (b) decay phases. The corresponding flux density increase (decrease) is from (to) 25% of its maximum value. The total number of bursts used in the distributions is 24 in (a) and 34 in (b). Here $\nu_{\rm pk}$ is taken at the peak time of $S_{\rm pk}(t)$.

positive shifts on the decay phase, which is not explained within the framework of the GS self-absorption model.

For the following analysis we will divide the events into three groups: those with high ($|\Delta\nu_{\rm pk}/\nu_{\rm pk}| \geq 0.3$)), moderate ($0.1 \leq |\Delta\nu_{\rm pk}/\nu_{\rm pk}| < 0.3$), and low ($|\Delta\nu_{\rm pk}/\nu_{\rm pk}| < 0.1$) relative peak frequency shifts and discuss them in detail below. Our aim is to show that, despite the wide variety of behavior, the different classes of events can be interpreted in terms of two competing effects, GS self-absorption and Razin suppression.

3.2. Peak Frequency Evolution on the Rising Phase of Bursts

3.2.1. Large Peak Frequency Shifts

In Figure 6 we show the correlation between $\nu_{\rm pk}$ and $S_{\rm pk}$ on the rising phase of the seven events with the highest relative peak frequency shifts, $\Delta\nu_{\rm pk}/\nu_{\rm pk} > 0.3$). The straight lines are the best linear fits (in logarithmic scale) near the peak of the bursts. Generally, we can see that the dependence is a power law

$$\nu_{\rm pk} \propto S_{\rm pk}^{\beta} \tag{7}$$

with the index β varying from event to event. The values of β for each event are listed in Table 1. As we can see the mean value of β is 0.27.

For comparison, in Table 1 we show also the power law indices β_1 and β_2 obtained for the fluxes at the previously defined frequencies ν_1 and ν_2 (see Equation (2)), below and above the peak. The mean values are $\beta_1 = 0.41$ and $\beta_2 = 0.19$. We can understand the differences between β, β_1 and β_2 in the context of self-absorption. Indeed, the value of β_2 is minimal, and β_1 is maximal, since in the

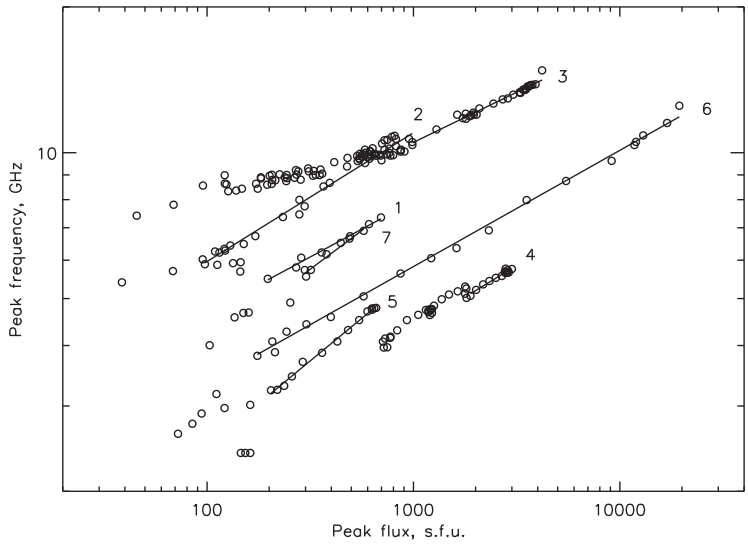

Figure 6. Peak frequency vs. peak flux density on the rise phase of seven events. The straight lines are the best linear fits (in logarithmic scale) near the peak of the bursts. The numbers indicate the events: 1–22 Apr 2001, 2–19 Oct 2001, 3–22 Oct 2001, 4–04 Nov 2001, 5–22 Nov 2001, 6–15 Jul 2002, 7–04 Dec 2002.

Table 1. Regression coefficients for events with $\Delta\nu_{\rm pk}/\nu_{\rm pk} > 0.3$.

Event	$\beta(\nu_{\rm pk}, S_{\rm pk})$	$\beta(\nu_{\rm pk}, S_2)$	$\beta(\nu_{\rm pk}, S_1)$
22 Apr 2001	0.23	0.14	0.30
19 Oct 2001	0.27	0.17	0.31
22 Oct 2001	0.21	0.18	0.27
04 Nov 2001	0.26	0.20	0.34
22 Nov 2001	0.34	0.27	0.66
15 Jul 2002	0.26	0.17	0.43
04 Dec 2002	0.32	0.22	0.54
Mean	0.27	0.19	0.41

optically thin regime the GS flux variations are expected to be much greater than in the optically thick regime under variations of the parameters like n, L, δ or B. The value of β falls between these limits, because flux density $S_{\rm pk}$ is from a partly optically thick, partly thin source with optical depth $\tau \simeq 1$.

Quantitatively the value of β also corresponds well with Equation (4) under the assumption that the area A, spectral index δ and magnetic field B do not change during the rising phase of these bursts. For electron spectral index $\delta = 2.0$–6.0, the theoretical value $\tilde{\beta} = 1/(2.50 + 0.085\delta) = 0.37$–$0.33$ is slightly greater than β, giving a mean difference $\tilde{\beta} - \beta = 0.08$. This slight but systematic reduction in β seems to arise from the approximate nature of Equation (4), since $S_{\rm pk}$ is actually formed at higher opacity than $\tau \approx 1$. Indeed, our simulations in Section 4.2 confirm that the GS shift in $\nu_{\rm pk}$ is slightly less than given by Equation (4).

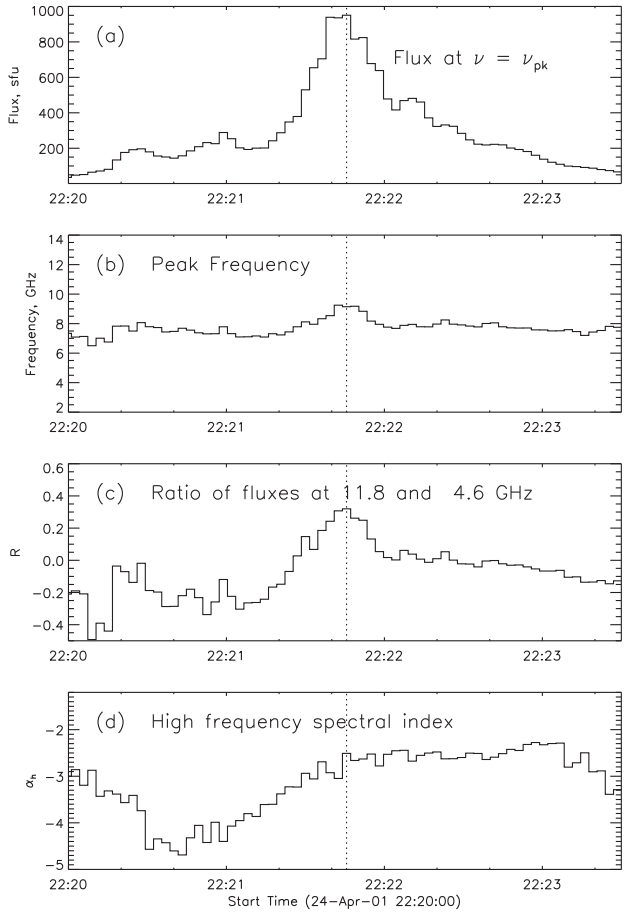

Figure 7. Time profiles as in Figure 3 for the burst of 24 April 2001. The peak frequency in (b) remains high and nearly constant except near the main peak in (a). The ratio R in (c) also becomes high and constant during the decay. Note that the spectral index $\alpha_{\rm h}$ in (d) increases all during the rise phase and is constant in most of the decay phase.

3.2.2. Moderate Peak Frequency Shifts: Time Delays

Our comparative analysis of the flux and peak frequency time profiles for the eight bursts that show moderate $0.1 < \Delta\nu_{\rm pk}/\nu_{\rm pk} < 0.3$ show that the bursts can be divided into two subsets according to the temporal behavior of $\nu_{\rm pk}$.

The first subset is characterized by relatively high and stable values of the peak frequency in the very beginning of the rising phase. The peak frequency starts to increase only after some delay relative to the flux increase, and peaks simultaneously (within the 4 s time resolution of OVSA) with the flux maximum. An example of such behavior is shown in Figures 7(a) and (b). Here $\nu_{\rm pk}$ maintains a relatively high and constant value during the entire burst. Only near the very peak does it slightly increase, with $\Delta\nu_{\rm pk}/\nu_{\rm pk} = 0.21$. We suggest that such behavior is indicative of Razin suppression, and will consider the effect in detail in Section 4.

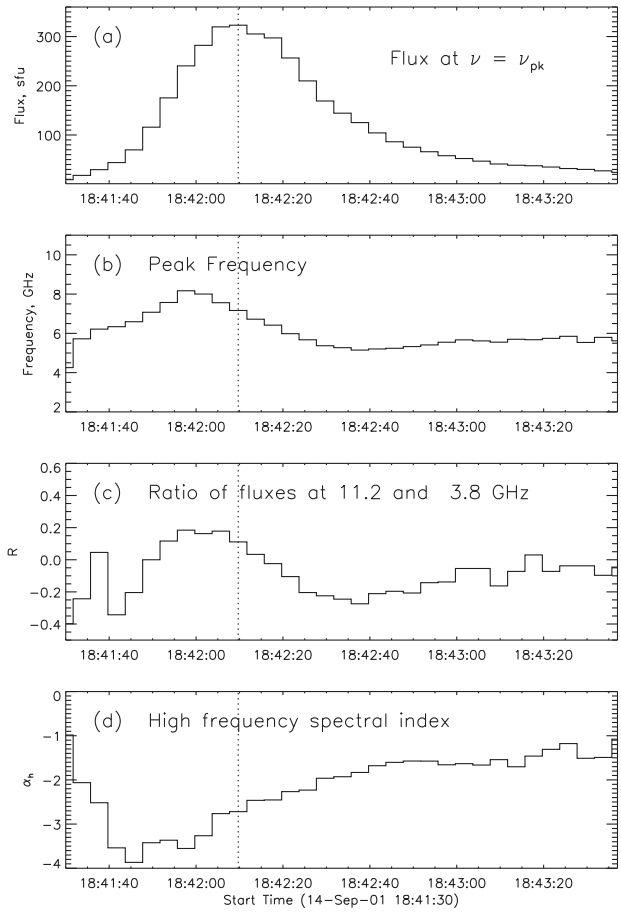

Figure 8. Time profiles as in Figure 3 for the bursts of 14 Sep 2001. This example shows a time delay between $\nu_{\rm pk}$ in (b) and $S_{\rm pk}$ in (a). Note also that on the decay $\nu_{\rm pk}$ first decreases and then slightly increases. The $\alpha_{\rm h}$ in (d) increases throughout the burst.

The second subset of events in this category is characterized by $\nu_{\rm pk}$ reaching its maximum value prior to the peak time of $S_{\rm pk}$, as shown in Figure 8. For these events, the peak frequency increases at a regular rate in the beginning of a burst, but then decreases prior to and throughout the peak of the burst. Note that the behavior of R in Figure 8(d) shows a similar time behavior. Such time delays also occur for events with small $\Delta\nu_{\rm pk}/\nu_{\rm pk}$ discussed in the next section. As a whole we found 10 events out of 24 where such time delays occur. The key to understanding this behavior, we believe, is that all of them show a significant increase (flattening) in $\alpha_{\rm h}$, which corresponds to a systematic flattening in the electron energy index δ. Flattening (steepening) of the electron spectrum over time can also cause the maximum value for $\nu_{\rm pk}$ to occur after (before) the flux density maximum.

Note that it is quite common for radio spectra to flatten during the decay phase of bursts, in apparent contradiction to the soft-hard-soft behavior most often seen in hard X-rays. The soft-hard-harder radio behavior and its relationship to hard

X-rays has been examined in detail by Melnikov and Silva (2000) and Silva, Wang, and Gary (2000), where the differences are ascribed to the fact that hard X-rays reflect the precipitating component, while the radio spectrum reflects the trapped component. When the trapped (looptop, or coronal, source) component can be isolated in hard X-rays (Krucker *et al.*, 2008), it is found to have a significantly harder spectrum than the footpoint source. Although both may derive from the same injected population (*e.g.* (Klein, Trottet, and Magun, 1986)), they evolve differently. Differences in electron spectral behavior derived from the radio spectrum relative to that derived from hard X-rays from footpoint sources should not be seen as a conflict. For our purposes, it is the trapped component, reflected in the high-frequency radio spectral slope, that is of interest.

To show that the flattening or steepening of the electron energy spectrum can affect the evolution of $\nu_{\rm pk}$ to such an extent as to cause these differences in timing, in Figure 9 we show the results of a simulation. We used the relation $\alpha_{\rm h} = 0.90\delta - 1.22$ from Dulk and Marsh (1982), for three different linear variations in electron spectral index, $\Delta\delta = -1,\ -0.5,\ +0.5$ and a gaussian time profile of nL. These variations of δ correspond to microwave slope variations of $\Delta\alpha_{\rm h} = +0.9, +0.45, -0.45$. It is clearly seen that hardening or softening of the electron spectrum affects the time of maximum of $\nu_{\rm pk}$ in the way indicated by the observations.

3.2.3. Small Peak Frequency Shifts

A total of nine bursts show small ($-0.1 < \Delta\nu_{\rm pk}/\nu_{\rm pk} < 0.1$) relative peak frequency shifts on their rise phase. Of these, five show complex behavior despite our attempt to choose only simple bursts. An example is the event of 2001 Aug 31 (not shown), where a burst with a simple flux density profile nevertheless displays a complicated shift of $\nu_{\rm pk}$, decreasing rapidly in the beginning before showing a more normal behavior through the peak. Such behavior may be a result of some previous burst activity or a radical source shift from a region of strong magnetic field to the one with weak magnetic field. We do not consider these events further.

The remaining four bursts with small $\Delta\nu_{\rm pk}/\nu_{\rm pk}$ are characterized by a nearly constant $\nu_{\rm pk}$ right through the flux density peak, while $S_{\rm pk}$ first increases and then decreases by a factor of several. Examples of two such events are shown in Figure 10. The constancy of the high frequency spectral index in both bursts indicates a constant electron spectral index δ, so it cannot influence the $\nu_{\rm pk}$ behavior. These bursts are relatively long and have smooth, gradual profiles. In fact, both bursts are secondary components of earlier, strong multi-component bursts. We can see in both events that R is nearly constant as well, indicating that the flux density increases and decreases almost with equal rate both at low ($\nu < \nu_{\rm pk}$) and high ($\nu > \nu_{\rm pk}$) frequencies. As we mentioned earlier, this is an indication of optically thin emission on both sides of the spectral peak, which is a clear signature of Razin suppression. This is investigated in more detail in Section 4.3.

3.3. Peak Frequency Evolution on the Decay Phase of Bursts

In general, peak frequency evolution on the decay phase considerably differs from the evolution on the rising phase. The powerlaw dependence of $\nu_{\rm pk}$ on $S_{\rm pk}$ seen in the rise phase is observed typically only in the beginning of the decay phase. In the late decay phase, the opposite dependence (*i.e.* $\nu_{\rm pk}$ begins to increase again) is seen for a significant fraction of events.

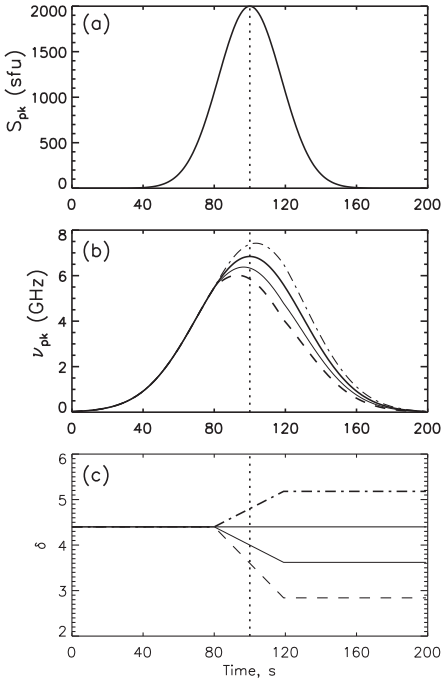

Figure 9. Simulation of the spectral evolution for (a) a Gaussian flux density profile under the influence of hardening or softening of the electron spectrum, (b) the leading or lagging of the time of maximum of $\nu_{\rm pk}$. The assumed electron spectral index evolution is shown in (c): solid line, δ =const; dashed line, $\Delta\delta = -0.5$; dotted line, $\Delta\delta = -1.0$; dot-dashed line, $\Delta\delta = +0.5$. The peak frequency time profile leads the flux maximum if the electron spectrum flattens, and it lags if the electron spectrum steepens.

3.3.1. Large Negative Frequency Shifts

Of the 34 bursts that we could study in the decay phase, there are 4 events with large negative relative frequency shifts, $\Delta\nu_{\rm pk}/\nu_{\rm pk} = -0.4$ to -0.6. In Figure 11 we show the relationship between $\nu_{\rm pk}$ and $S_{\rm pk}$ for these events. The straight lines are the best linear fits (in logarithmic scale) near the peak of the bursts. This dependence can be described by the same power law expression as Equation (7). The values of β for each of the four events are listed in Table 2. From the table we can see remarkably high values of slope β (average $\beta = 0.57$) relative to the value of $\beta = \tilde{\beta} \simeq 0.35$ expected from Equation (4), much higher than the highest values of β found during the rising phase of bursts (see Table 1).

Such a strong decrease of $\nu_{\rm pk}$ on the decay phase can be explained by one or more of the effects that we discussed earlier: increase of the source area A, flattening of the electron energy spectrum (decrease of δ), or decrease in magnetic field B.

Again, we cannot investigate the change of the magnetic field and area without spatially resolved observations, but we can use the observed microwave spectral index $\alpha_{\rm h}$ to investigate δ. First of all, we have found that $\alpha_{\rm h}$ does flatten on the decay phase of the bursts, giving $\Delta\alpha_{\rm h} = 1.8,\ 1.3,\ 1.3$, and 0.6 for the events 30 Aug 2001, 31 Aug 2001, 22 Oct 2001, and 28 Aug 2002, respectively. These correspond

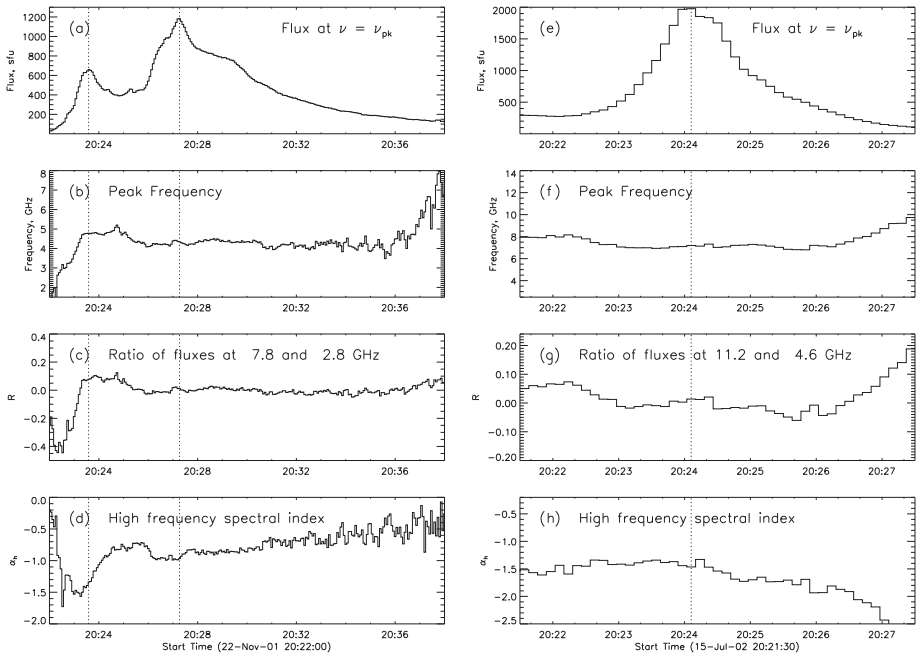

Figure 10. Time profiles as in Figure 3 for the second major peak of the bursts of 22 Nov 2001 (panels (a)-(d)) and 15 Jul 2002 (panels (e)-(h)). The peak frequency in both bursts (panels (b) and (f)) is remarkably constant during the main part of the rise and decay. The same is true for the ratio R (panels (c) and (g)). On the late decay phase the peak frequency starts to increase.

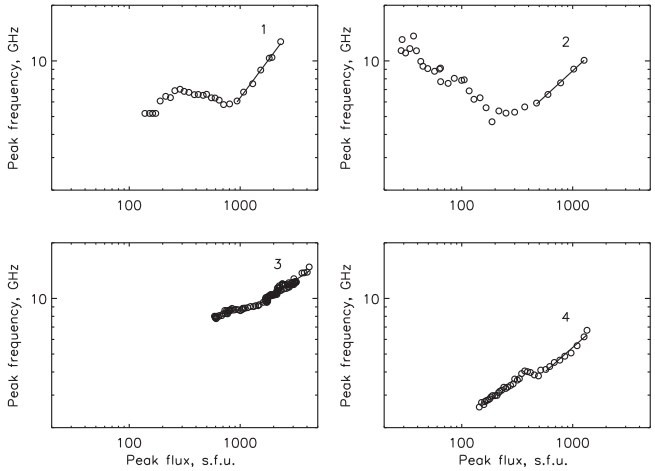

Figure 11. The relationship between the peak frequency, $\nu_{\rm pk}$, and peak flux density, $S_{\rm pk} = S(\nu_{\rm pk})$ on the decay phase of four events with the highest values of $\Delta\nu_{\rm pk}/\nu_{\rm pk}$. The straight lines are the best linear fits (in logarithmic scale) near the peak of the bursts. The numbers indicate the events: 1–30 Aug 2001, 2–31 Aug 2001, 3–22 Oct 2001, 4–28 Aug 2002.

Table 2. Regression coefficients for events with $\Delta\nu_{\rm pk}/\nu_{\rm pk} < -0.4$

Event	$\beta(\nu_{\rm pk}, S_{\rm pk})$	$\beta(\nu_{\rm pk}, S_{\rm thin})$	$\beta(\nu_{\rm pk}, S_{\rm thick})$
30 Aug 2001	0.80	0.45	> 0.78
31 Aug 2001	0.55	0.39	> 0.55
22 Oct 2001	0.39	0.32	> 0.52
28 Aug 2002	0.53	0.27	> 0.42
Mean	0.57	0.36	> 0.57

to $\Delta\delta = 2.0,\ 1.4,\ 1.4, 0.7$, respectively. These spectral index variations can explain a considerable part of the difference $\tilde{\beta} - \beta$, but not all of it. In our opinion, some of the enhanced decrease of $\nu_{\rm pk}$ must be ascribed to some other effect, such as the radio source shift into the looptop region with a weaker magnetic field (Melnikov *et al.*, 2002). We conclude that GS self-absorption can explain the four bursts with large negative peak frequency shifts, but only when other effects are included.

It is interesting that the opposite case, strong Razin suppression, can in some special circumstances also result in large negative shifts in $\nu_{\rm pk}$ on the decay. As shown in Figures 8(c) and 8(d) of Bastian, Fleishman, and Gary (2007), a plausible combination of plasma heating (which lowers free-free opacity) and a drop in density of high-energy particles may result in an arbitrarily high $\beta(\nu_{\rm pk})$, *i.e.* a decrease in $\nu_{\rm pk}$ at nearly constant $S_{\rm pk}$.

3.3.2. Moderate Negative Frequency Shifts

A total of 12 events show relative shifts ($-0.3 < \Delta\nu_{\rm pk}/\nu_{\rm pk} < -0.1$). Six of these are chosen for illustration and listed in Table 3. These bursts have mean value $\beta \simeq 0.4$ that is closer to the theoretical expectations. The detailed analysis shows that in some cases the moderate values of $\Delta\nu_{\rm pk}/\nu_{\rm pk}$ are actually large-shift events whose overall slope is moderated due to a change of the evolution from an initial steep decrease to a constant or increasing value of $\nu_{\rm pk}$ on the time interval over which the slope is measured. Such a change in slope during the decay is quite typical. In fact, in only 4 of the 12 events did the peak frequency decrease monotonically. In the other 8 events the peak frequency initially dropped quickly, but became constant or started to increase before $S_{\rm pk}$ had dropped by an order of magnitude. We will discuss these flat or increasing frequency shifts on the decay shortly.

3.3.3. Small Frequency Shifts

Eleven events show small relative frequency shifts on the decay, in the range $-0.1 < \Delta\nu_{\rm pk}/\nu_{\rm pk} < 0.1$. About half of these bursts (6 of 11) are explained by a similar change of slope of $\nu_{\rm pk}$ vs $S_{\rm pk}$ that we saw in the previous section, from an initial decrease to a later increase. In the other five events we observe small, gradual monotonic shifts or even remarkably flat values of $\nu_{\rm pk}$ on the decay phase similar to what we have already discussed for the rising phase. The examples of such a behavior can be seen in Figure 10. For 7 of these 11 events the peak frequency became constant or started to increase before $S_{\rm pk}$ dropped by an order of magnitude (see Figure 11).

Table 3. Regression coefficients for events with $-0.3 < \Delta\nu_{\rm pk}/\nu_{\rm pk} < -0.1$.

Event	$\beta(\nu_{\rm pk}, S_{\rm pk})$	$\beta(\nu_{\rm pk}, S_{\rm thin})$	$\beta(\nu_{\rm pk}, S_{\rm thick})$
25 Aug 2001	0.95	0.52	1.97
28 Dec 2001	0.35	0.19	0.65
20 Jul 2001	0.21	0.16	0.38
26 Jul 2001	0.27	0.20	0.56
28 Aug 2002	0.27	0.20	0.43
31 Oct 2002	0.38	0.20	> 0.7
Mean	0.40	0.24	> 0.8

3.3.4. Positive Frequency Shifts

Despite the fact that GS self-absorption requires a decrease in $\nu_{\rm pk}$ during the decay phase, a large percentage (23 of 34 events, *i.e.*$\approx 68\%$) in our sample display a considerable *increase* of $\nu_{\rm pk}$ starting at some point during the decay phase. As we have already mentioned in Sections 3.3.1–3.3.3, in most cases the increase begins after some decrease of the burst flux, often by a factor of 2-3 and sometimes by a larger factor.

The characteristic time delay of the beginning of the peak frequency increase relative to burst maximum is 2 minutes. However, the delay varies considerably from event to event. In several events it begins just after the intensity peak, while in more than 1/3 of events it is quite long, varying from 2 to 8 minutes. These events are usually long lasting gradual bursts with relatively low peak frequency, $\nu_{\rm pk} \lesssim 7$ GHz, prior to the increase (see examples in Figure 10). In Figures 10(f) and (g) one can clearly see the considerable increase of $\nu_{\rm pk}$ and ratio R on the late decay phase, starting from 20:26 UT. The increase of R means that the flux decrease at low frequency $\nu_1 = 4.6$ GHz $< \nu_{\rm pk}$ goes faster than at high frequency $\nu_2 = 11.2$ GHz $> \nu_{\rm pk}$. The faster flux decrease at lower frequencies (steepening of the spectrum at $\nu < \nu_{\rm pk}$) after moment t_6 is easily seen in Figure 2(c), which is the same burst as in Figures 10(e)–(h). Note that the shape of the microwave spectrum during this increase remains the typical GS spectrum with a well pronounced spectral peak.

We have examined possible reasons for an increase in $\nu_{\rm pk}$ in the late decay phase, such as thermal GS emission, or variations in parameters (decrease in A, or increase in B), and again find that the most plausible explanation is an increase in density in the decay phase, which increases the effect of Razin suppression with time. A further analysis of this possibility will be given in the next section.

4. Model Simulations

We showed earlier that in a majority of bursts the peak frequency shifts are well correlated with flux density (at least near the maximum of the burst), as expected if the spectral turnover is due to GS self-absorption. We also showed that other effects such as evolution of the electron energy distribution can act in concert with

GS self-absorption to account for some other peculiarities of spectral dynamics (*e.g.* time delays between $\nu_{\rm pk}$ and $S_{\rm pk}$).

However, GS self-absorption cannot explain behavior found in a significant number of events including: 1) slight variations or even constancy of the peak frequency even when the burst intensity changes by an order of magnitude or more, or 2) a shift of the peak frequency to higher frequencies starting in the middle or late decay phase. A common feature that seems associated with the above behavior is a relatively low maximum value for $\nu_{\rm pk}$. In some events $\nu_{\rm pk}$ can be as small as 3 GHz, which indicates a relatively weak magnetic field in the radio source. In this section we will examine Razin suppression as a mechanism to explain each of these properties.

One of the main observational clues of the existence of Razin suppression that has been cited in the literature is the steep low-frequency total power spectra expected from a homogeneous source. With rare exceptions, our events do *not* show such steep spectra. But it is well known that steep low-frequency spectra are expected in total power only for the case of a homogeneous source, whereas typical flares display considerable inhomogeneity that we argue will destroy this signature of Razin suppression. In the Appendix we present a simple model to demonstrate the effect. Inhomogeneity, of course, may also affect the evolution of the peak frequency, as we mentioned in the previous sections. Nevertheless, to avoid unnecessary complication and to show the pure effect of Razin suppression on the microwave spectral dynamics, in the following models the magnetic field and plasma density are homogeneous in the microwave source.

4.1. Gyrosynchrotron Spectrum Formation

The idealized GS spectrum has a single peak at $\nu = \nu_{\rm pk}$ whose low frequency turnover is either due to GS self-absorption (Twiss, 1954) or due to Razin suppression (Razin, 1960a,b). In the GS self-absorption case, the peak frequency occurs near optical depth unity:

$$\tau(\nu_{\rm pk}) = \kappa_\nu L \approx 1, \tag{8}$$

where κ_ν is the absorption coefficient, and L is the source thickness. In the case of Razin suppression (for classical synchrotron emission) the low frequency turnover is associated with the Razin frequency:

$$\nu_{\rm R} = \frac{2\nu_{\rm p}^2}{3\nu_B}, \tag{9}$$

where $\nu_{\rm p}$ and ν_B are the plasma frequency and gyrofrequency, respectively. So it is proportional to the ratio of plasma number density to magnetic field strength. High ambient density and/or low magnetic field strength act to raise $\nu_{\rm R}$.

In this section, we carry out numerical simulations of peak frequency dynamics for homogeneous sources using the exact formalism for the GS emissivity and absorption coefficient (Ramaty, 1969, 1994). Electrons in the source are assumed to have a power law distribution and to be distributed isotropically. The time profile of nonthermal electrons is chosen to have a Gaussian shape with effective duration and maximum time defined by the values t_0 and $t_{\rm m}$, respectively:

$$n(E,t) = k\ \exp\Big[-\frac{(t-t_{\rm m})^2}{t_0^2}\Big] E^{-\delta}, \tag{10}$$

where E is the electron energy in MeV in the range 0.01-500 MeV, δ is electron spectral index, and k is a constant factor. We consider cases with low and high plasma density, with constant and varying electron energy power law index, and a case in which the plasma density increases with time.

4.2. Influence of Self-Absorption

Figure 12 displays the spectral evolution of GS emission in a low density plasma, for parameters such that the low frequency turnover is entirely determined by GS self-absorption and Razin suppression is almost negligible at $\nu \geq 2$ GHz. The increase of GS intensity on the rise phase occurs due to the increase in number of energetic electrons and leads to the corresponding increase of $\nu_{\rm pk}$ (panels (a) and (d)). On the decay phase, the behavior is symmetrical. Note the low initial value ($\nu_{\rm pk}$ can be as low as 1.2 GHz) and large range of peak frequency variations: $\nu_{\rm pk}$ changes by a factor of two when $S_{\rm pk}$ changes by an order of magnitude. Note also a strong change (two orders of magnitude) in the ratio of fluxes, R, at high $\nu_2 > \nu_{\rm pk}$ and low $\nu_1 < \nu_{\rm pk}$ frequencies (defined after Equation (2)), which occurs due to very small variation of the flux at ν_1 where the source is optically thick. Panel (c) shows the dependence of the peak frequency on the peak flux as in Figure 6. The dependence is roughly a power law, $\nu_{\rm pk} \propto S_{\rm pk}^{\beta}$ with $\beta = 0.27$, in agreement with the observations (Figure 6) and lower than the prediction from Equation (4) obtained from the simplified formulas for GS emission by Dulk and Marsh (1982). The behavior in Figure 12 looks similar to that of the event in Figure 1.

4.3. Influence of High Plasma Density: Razin Effect

When the ratio of plasma density to magnetic field in a source is large (the plasma parameter $Y = \nu_{\rm p}/\nu_B \gg 1$), the GS spectrum is strongly influenced by the ambient medium. For relativistic electrons, this effect is known as Razin suppression, and modifies the spectrum to produce an exponential decrease of the emissivity and absorption coefficient at low frequencies, $\nu < \nu_{\rm R}$ (Razin, 1960a), and considerable flattening of the original synchrotron power law spectrum, $S_\nu \sim \nu^{-\alpha}$, at higher frequencies (Razin, 1960b).

The physical meaning of the influence of the medium can be understood from the simple consideration of Lienard-Wiechert potentials $\mathbf{A}$ and ϕ in a medium with index of refraction $n < 1$ (Ginzburg, 1953):

$$\mathbf{A}(t) = \left[\frac{ev}{c(r - n\mathbf{r}\cdot\mathbf{v}/c)}\right]_{t-n\frac{r}{c}} \tag{11}$$

$$\phi(t) = \left[\frac{e}{n^2(r - n\mathbf{r}\cdot\mathbf{v}/c)}\right]_{t-n\frac{r}{c}}, \tag{12}$$

where e is the electron charge, and $\mathbf{r}$ is the radius-vector of the electron moving with velocity $\mathbf{v}$ taken at the retarded time $t' = t - nr/c$. It follows from Equations (11) and (12) that the emissivity of a single electron depends strongly on the ratio of the electron velocity v to the wave phase velocity $v_{\rm ph} = c/n$. In vacuo, $n = 1$ and therefore the effectiveness of emission is very high when the electron velocity is close to the speed of light c, since the denominator in Equations (11) and (12)

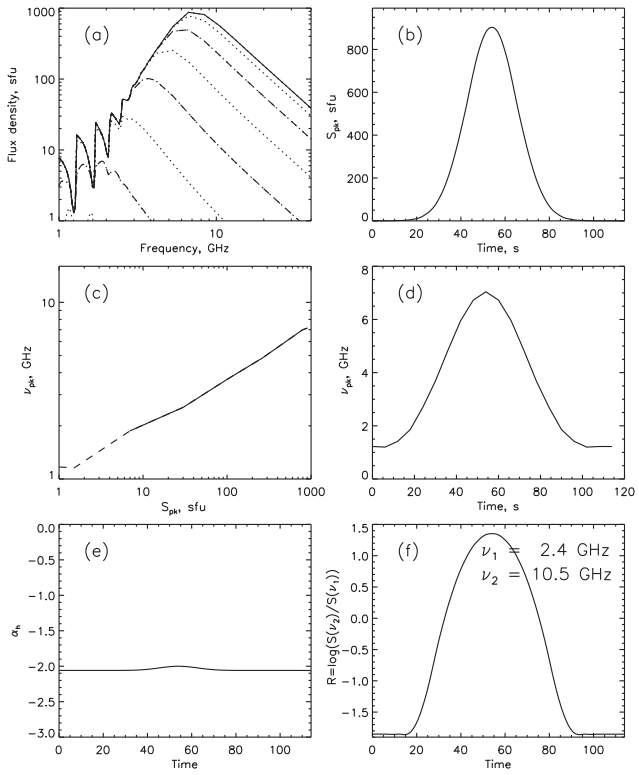

Figure 12. Spectral evolution of GS emission in a low density plasma ($n_0 = 5 \times 10^9$ cm^{-3}, $B = 150$ G, $t_m = 54$ s, $t_0 = 12$ s, $\delta = 4.0$, $L = 10^9$ cm, $\phi = 17''$, $k = 10^4$). For these parameters, the low frequency turnover is determined by GS self-absorption. Panel (a): Flux density spectrum at different times on the rising (dotted lines) and decay (dashed lines) phases. Panel (b): Peak flux time profile $S_{pk} = S(\nu_{pk})$. Panel (c): Dependence of the peak frequency on the peak flux on a log scale (solid and dashed lines for the rise and decay, respectively). Panel (d): Peak frequency evolution. Panel (e): High frequency spectral index evolution. Spectral index is defined by fitting of a calculated spectrum (panel (a)) at frequencies $\nu > \nu_2$, $\nu_2 = 1.5\nu_{pabs}$ (see Equation (2)). Panel (f): Evolution of logarithm of the flux ratio R at $\nu_2 > \nu_{pk}$ and $\nu_1 < \nu_{pk}$.

tends to 0. In a plasma, $n < 1$ and the denominator can never be very close to 0, even if $v \simeq c$. So a relativistic electron has an emission efficiency comparable with a nonrelativistic one, *i.e.* much lower than in vacuo. This causes a strong suppression of radiation in the plasma, especially at lower frequencies since in plasma $n^2 \simeq 1 - \nu_p^2/\nu^2$. The Razin effect is predominantly a relativistic effect. As follows from Equations (11) and (12), the strong influence of the refraction coefficient n is only possible if the electron velocity v is close to the speed of light c.

Figure 13 shows the spectral evolution of GS emission for relatively high plasma density $n_0 = 5 \times 10^{10}$ cm^{-3}. The other parameters in the source are the same as in Figure 12. In the beginning of the rise phase and during the late decay phase the radio source is optically thin at low frequencies due to the Razin effect. Due to the high ratio of n_0/B, the values of ν_{pk} are quite high, ≈ 5 GHz. Although the flux density is changing, the peak frequency remains nearly constant during these

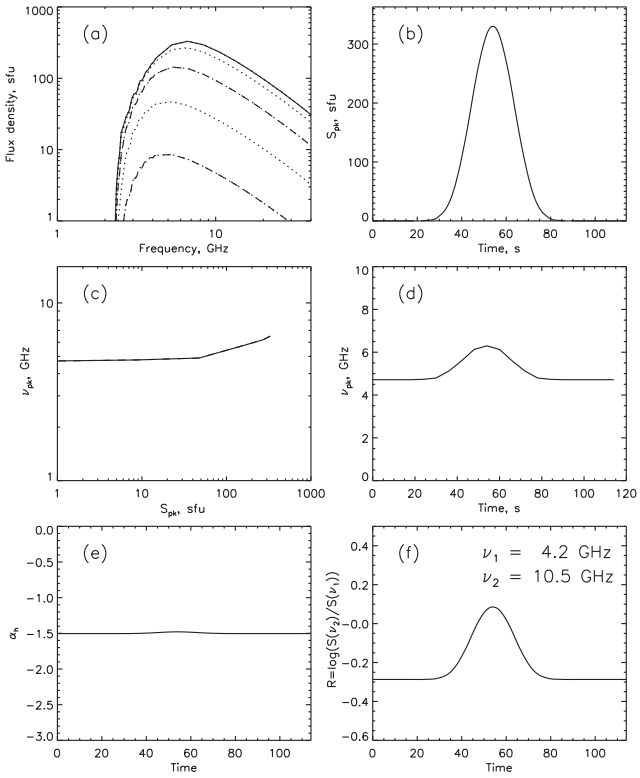

Figure 13. Spectral evolution of GS emission in the presence of high density plasma: $n_0 = 5 \times 10^{10}$ cm^{-3}. The other parameters are same as in Figure 12. The low frequency turnover is determined by two effects: 1) by the Razin suppression on the initial rising phase and late decay phase, and 2) by the self-absorption near the maximum of the simulated burst. Note the high initial value and small range of the peak frequency and R variations.

periods. The low and high frequency fluxes change nearly at the same rate leading to R =const. However, near the maximum of $S_{\rm pk}$, when the column density of nonthermal particles becomes high enough, the source becomes optically thick at $\nu \leq \nu_{\rm pk}$, despite the Razin suppression, and the spectral evolution of $\nu_{\rm pk}$ follows the familiar behavior where the self-absorption plays the main role. Note, however, the reduced range of this peak frequency variation, only about $\approx 30\%$ for an order of magnitude change in $S_{\rm pk}$. The variation of R (< 0.5 order of magnitude) is also considerably smaller than in the case of pure self-absorption (Figure 12). The slope of $\nu_{\rm pk}$ vs. $S_{\rm pk}$ is much flatter than in the absence of the Razin suppression, with $\beta < 0.17$. This is comparable to the values of β found for the events with moderate $\Delta\nu_{\rm pk}/\nu_{\rm pk}$ (see Section 3). It is clear that for smaller k (defining the number density of energetic electrons, Equation (10)) the amplitude of the $\nu_{\rm pk}$ variation and the value of β will decrease. With sufficiently small k, we get no visible change at all in $\nu_{\rm pk}$. Another remarkable feature of the case with high plasma density (high level of Razin suppression) is a flatter high-frequency spectral slope at $\nu > \nu_{\rm pk}$. It follows from Figures 12(e) and 13(e) that the difference in the spectral indices is 0.5.

The spectral evolution shown in Figure 13 is similar to the $\nu_{\rm pk}$ evolution in Figure 7. Bursts with this spectral evolution indicate the presence of considerable Razin suppression, and serve as a diagnostic of high plasma density to magnetic field ratio in flaring loops.

4.4. Razin Effect and Electron Power Law Index

We show in Figure 14 the spectral evolution when both spectral hardening and Razin suppression are present. We expect a higher $\nu_{\rm pk}$ for flatter electron spectra (lower δ). We assume a linear change of δ from 5 to 3 during the burst. To show the pure effect, here we have set the number density of energetic electrons sufficiently low that GS self-absorption is never important, even near the burst maximum. As expected, the peak frequency increases throughout the rising and decay phases while the electron energy spectrum continuously hardens (panel (d)). While δ changes from 5 to 3, the peak frequency increases from 3.5 up to 8 GHz. The steepest increase of $\nu_{\rm pk}$ occurs in the late decay phase, where the electron spectrum is hardest. Note also the considerable increase of the flux ratio during the burst: almost an order of magnitude (panel (f)). This happens since at both frequencies, ν_1 and ν_2, the source is optically thin. Therefore, due to the electron spectral hardening the flux at low frequency increases slower on the rise phase of the burst and decreases faster on the decay phase.

Finally, in Figure 15 we add the effect of GS self-absorption by increasing of the number density of energetic electrons by a factor of 10 relative to the case shown in Figure 14. As we saw earlier, the behavior is modified near the peak of the burst due to a temporary increase of the optical thickness of the GS source. At other times, Razin suppression is dominant in defining the spectral peak. Note that the $\nu_{\rm pk}$ and R on the decay phase (panels (c)–(f)) are always higher than on the rising phase similar to the observed behavior described in Section 3.3.4.

4.5. Plasma Density Increase on the Late Decay Phase

An energy release of sufficient magnitude in a flaring loop will be accompanied by chromospheric evaporation, which will increase the plasma density inside the loop over time. As we have shown, such an increase, if it is great enough, may produce a gradual increase of $\nu_{\rm pk}$ in the middle or late decay phase as the Razin effect becomes dominant.

A simulation of this process is shown in Figure 16. We suppose that the plasma density in the loop starts to increase at the burst maximum and increases throughout the decay phase. Near the burst maximum, the dominant low frequency turnover mechanism is GS self-absorption, but on the late decay phase the Razin effect dominates. This is shown by the fact that the flux at low and high frequencies changes almost at the comparable rate (see panel a, dashed lines). On panels (c) and (d) one can see that just after the flux maximum the peak frequency decreases more slowly than on the rising phase ($\beta = 0.02$) and then starts to increase. To get a 2 GHz increase of $\nu_{\rm pk}$ as shown on the panel (d), we need only a 50% plasma density enhancement. It is interesting to note that the high frequency spectral index also increases (spectrum flattens) along with the plasma density on the decay phase (panel (e)). This occurs due to the already mentioned effect of the medium at high frequencies, $\nu > \nu_{\rm pk}$ (Razin, 1960b). Note that this is only true in

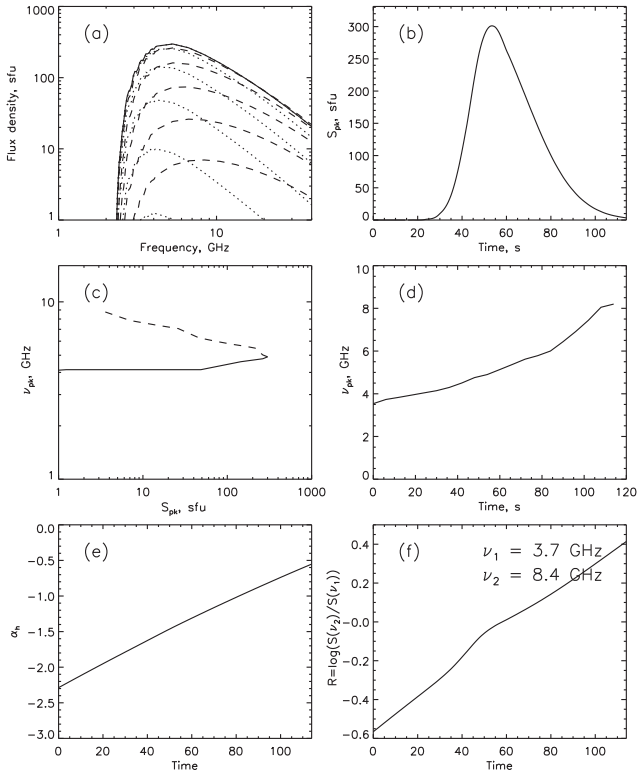

Figure 14. Spectral evolution of GS emission in the presence of high density plasma and continuous electron spectrum hardening, $\delta = 4.0 - (t - t_{\max})/t_{\max}$. The other parameters are the same as in Figure 13 except $k = 10^3$ and $\phi = 45''$. Note the continuous increase of $\nu_{\rm pk}$ and R on the rise and decay phases. On panels (a) and (c) solid line is for the rising phase and dashed line for the decay phase.

the restricted frequency range considered here. Asymptotically at large frequencies the spectral index does not change.

We should say that a similar $\nu_{\rm pk}$ increase occurs if the magnetic field in the radio source gradually decreases on the late decay phase. To get the same enhancement of $\nu_{\rm pk}$, we need only 25% decrease of the magnetic field strength. In principle this can happen as newly reconnected loops appear at higher levels in the corona during continuous energy release and particle acceleration in the helmet coronal structures.

5. Discussion and Conclusion

Dynamical changes in the peak frequency of the GS spectrum of microwave bursts have been analyzed using data on 338 bursts obtained in 2001–2002 with OVSA. We find that the dynamical changes show a few distinct behaviors, which we have interpreted in terms of two competing effects: a) GS self-absorption and b) Razin suppression.

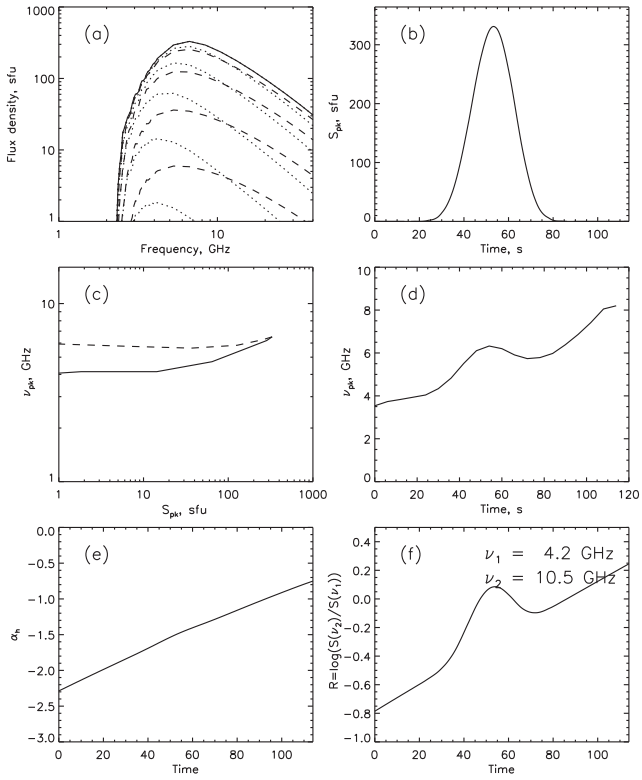

Figure 15. Spectral evolution of GS emission in the presence of high density plasma and electron spectral hardening, $\delta = 4.0 - (t - t_{\max})/t_{\max}$. The other parameters are the same as in Figure 13. The increase and decrease of $\nu_{\rm pk}$ and R in the main part of the emission peak is due to GS self-absorption. A new increase of the peak frequency and the flux ratio with time is clearly seen on the decay phase when the source becomes optically thin at low frequencies and the Razin suppression becomes dominant in defining the spectral peak.

Observationally we find that, for a majority of a subset of 38 simple bursts, the peak frequency is very well correlated with the intensity of microwave bursts, at least near the burst maximum. The peak frequency increases on the rise phase in $\approx 83\%$ of 24 bursts where it could be cleanly measured, and decreases on the decay phase in $\approx 62\%$ of 34 bursts, in qualitative agreement with GS self-absorption as the origin of the low frequency turnover of the spectrum. For some bursts of this type, however, we find a faster than expected decrease of $\nu_{\rm pk}$ on the decay phase. This behavior is correlated with flattening of the high-frequency slope (increasing $\alpha_{\rm h}$) of the microwave spectrum, which is indicative of hardening of the electron energy distribution. The presence in many bursts of a positive or negative time difference between the maxima of $\nu_{\rm pk}$ and $S_{\rm pk}$ time profiles is also shown to be due to GS self-absorption under evolution (usually hardening but sometimes softening) of the electron spectral index.

However, we also find that for ≈30-36% of bursts the peak frequency increase near the burst maximum is much smaller than expected or even may be entirely absent. Typically in these bursts $\nu_{\rm pk}$ starts at a rather high frequency in the very

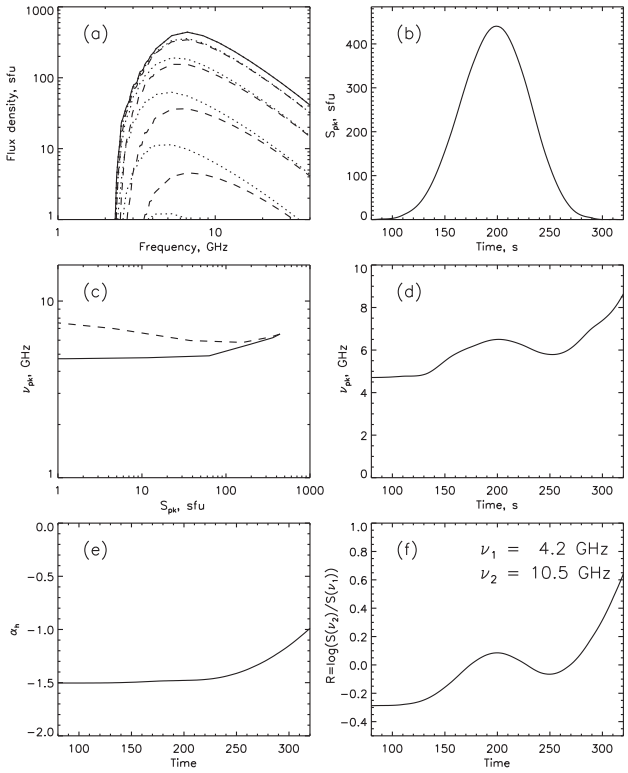

Figure 16. Spectral evolution of GS emission in the case of plasma density increase on the decay phase: $n(t) = n_0[1 + 2(t - t_m)^2/t_m^2]$, where $n_0 = 5 \times 10^{10}$ cm$^-3$, $t_m = 200$ s. The other parameters are the same as in Figure 13, except $\phi = 20''$. The increase of ν_{pk}, R and α_h on the late decay phase is completely due to the influence of high plasma density (Razin effect).

beginning of the burst and remains almost constant during a considerable (factor of ≈ 10) increase and decrease of the burst intensity. We explain this temporal behavior as follows: In the beginning of the rise phase and during the late decay phase the radio source is optically thin at low frequencies due to the Razin effect. But briefly near the maximum, when the column density of nonthermal particles becomes high enough, the source becomes nearly optically thick at $\nu \leq \nu_{pk}$, despite the Razin suppression, and the spectral evolution of ν_{pk} takes on the characteristics for GS self-absorption.

About 70% of bursts show a gradual increase in ν_{pk} starting at some point in the decay phase. We show that this behavior can easily be explained by Razin suppression together with either hardening of the high energy electron spectrum or an increase in Razin parameter (due to an increase in plasma density or a decrease in magnetic field strength in the microwave source). Again, the evidence for electron spectral hardening, when present, can be obtained directly from the observed flattening of the microwave high frequency spectral slope. An increase in ν_{pk} in the late phase that is unaccompanied by microwave spectral flattening may thus be a direct signature of chromospheric evaporation and/or evolution of the source to greater heights where the magnetic field strength is lower.

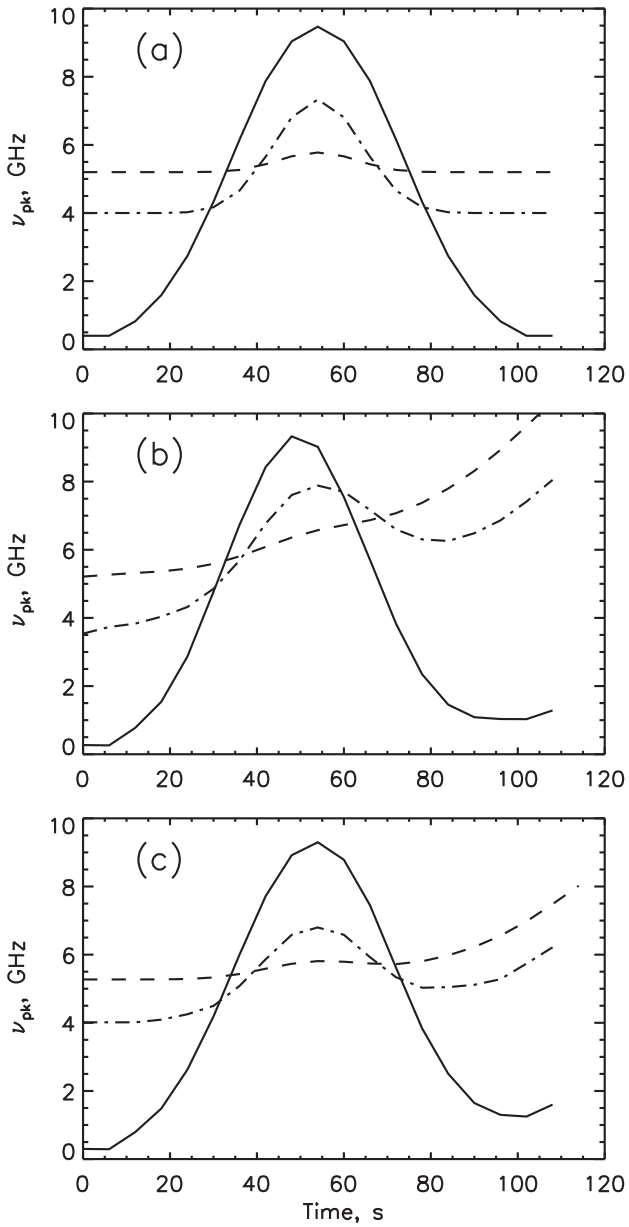

Figure 17. Schematic representation of characteristic time profiles of the peak frequency expected from GS theory. The three curves in each panel are (solid line) self-absorption dominant throughout a burst, (dot-dashed line) Razin suppression dominant in the beginning and end of a burst, but self-absorption important near the burst maximum, and (dashed line) Razin suppression dominant throughout a burst. The panels show three cases: (a) electron spectral index is constant, (b) continuous hardening of the electron spectrum, (c) stable electron index but Razin suppression (as expressed by $Y = \nu_{\rm p}/\nu_B$) increases on the decay phase.

Using numerical calculations from GS theory, including the effect of the medium, we have confirmed that the wide range of evolutionary behavior can be interpreted as an interplay between GS self-absorption and Razin suppression. In Figure 17 we show a schematic representation summarizing our theoretical predictions. The time profiles of $\nu_{\rm pk}$ are shown in each panel for three cases: 1) GS self-absorption is dominant throughout the burst (solid lines), 2) Razin suppression is dominant in the beginning and end of the burst, while GS self-absorption is important near the burst maximum (dot-dashed lines), 3) the Razin suppression is dominant throughout the burst (dashed lines). These three cases correspond to increasing values of parameter $Y = \nu_{\rm p}/\nu_B$ from low to moderate to high. Figure 17(a) shows the case when other parameters are held constant; Figure 17(b) for the case of continuous hardening of the electron spectrum, which can be recognized from the evolution of $\alpha_{\rm h}$; and Figure 17(c) for the case when the electron spectrum is stable but the parameter $Y = \nu_{\rm p}/\nu_B$ increases on the decay phase of the burst.

Applying these theoretical predictions to our observational findings, we can say that Razin suppression plays an important role in the spectral dynamics of more than 70% of bursts, at least on their decay phase. For the Razin effect to be important for a relatively large number of bursts (with average $\nu_{\rm pk} \approx 6$ GHz), we require that the magnetic field in the source be relatively weak (100–300 G for a corresponding plasma density 1–10 $\times$ 10^{10} cm^{-3}). Now that we have shown how to recognize the presence of Razin suppression from the dynamical changes in $\nu_{\rm pk}$ and R during a burst, the changes in $\nu_{\rm pk}$ can be used quantitatively as a further constraint on the evolution of plasma parameters, especially ambient density and magnetic field strength. Together, the combination of spectral measures (1) temporal evolution of $\nu_{\rm pk}$, (2) R, the logarithm of the ratio of flux densities above and below $\nu_{\rm pk}$, and (3) the high-frequency slope $\alpha_{\rm h}$, relative to the flux density at spectral maximum, $S_{\rm pk}$, provide a new, valuable diagnostic for microwave bursts of GS origin.

It is well known (Bastian, Benz, and Gary, 1998) that microwave burst sources typically have an inhomogeneous spatial structure. Inhomogeneous magnetic field, plasma density and high-energy electron distributions in these sources (see *e.g.* Klein and Trottet, 1984; Preka-Papadema and Alissandrakis, 1988; Simões and Costa, 2006) can considerably disturb the total microwave spectrum and its evolution. So, to be of greatest diagnostic power, the spectral dynamics should be measured in brightness temperature, *i.e.* using spatially resolved spectra. In this case the above theoretical predictions are more directly applicable since the inhomogeneity is only that along the line of sight. Such measurements require simultaneous spatial and spectral resolution over a wide band of frequencies. The work of Belkora (1997) and Melnikov *et al.* (2005) are the only published examples that showed Razin suppression in a brightness temperature spectrum. Such observations will be possible routinely with a new generation radio facility, the Frequency Agile Solar Radiotelescope (FASR), now under development. For more comprehensive application of these new diagnostics to flaring loops, such microwave data should be analyzed in combination with diagnostics from EUV, X-ray and gamma-ray data.

Acknowledgements The Owens Valley Solar Array and this work are supported by NSF grants AST-0607544 and ATM-0707319, and NASA grant NNG06GJ40G to New Jersey Institute of Technology. VM also acknowledges support by RFBR grants 06-02-39029, 06-02-16295, 07-02-01066 to Radiophysical Research Institute (NIRFI).

Appendix. Effect of Inhomogeneity on Razin Suppression

The effect of inhomogeneity on a total power spectrum is generally to flatten the low frequency slope. This effect can easily destroy the steep low frequency slope expected for Razin suppression. To show this, we present a simple model of a flaring loop that is inhomogeneous perpendicular to its axis, and consider the radio emission along a line of sight looking down through the top of the loop, as indicated in Figure 18(a). The loop axis height is taken to be $h = 6 \times 10^8$ cm, and we choose parameters for which the Razin frequency on the loop axis is $\nu_R = 20 n_e/B = 10$ GHz. Thus, we take the electron density at the apex to be $n_0 = 5 \times 10^{10}$ cm^{-3} and the magnetic field to be 100 G. To allow for inhomogeneity, we let the magnetic field vary slightly along the line of sight s, according to $B = 120(s_1/(s+s_1))^3$, with $s_1 = 9.6 \times 10^9$ cm. The electron density is taken to have a gaussian profile along the line of sight, with its maximum at the loop axis, $n_e = n_0 \ \exp\left[-(s-h)^2/s_0^2\right]$, where the $1/e$ width is $s_0 = 3.3 \times 10^8$ cm. Likewise, the high energy electron distribution across the loop is $N(E > 1 \text{ MeV}) = N_0 \ \exp\left[-1.7 \ (s-h)^2/s_0^2\right]$, where $N_0 = 1.1 \times 10^5$ cm^{-3}. The angle between the magnetic field and the line-of-sight is ≈ 78 degrees. The electron energy spectrum is given by a single power law in the range $E = 100 - 31600$ keV with the electron spectral index $\delta = 3.0$.

From this model employing quite reasonable parameters we obtain the spectrum in Figure 18(b). The emission at the peak frequency and higher frequencies comes mainly from the central (most dense) part of the loop, where the Razin effect suppresses the low frequency emission and forms the spectral peak. On the other hand, the emission at lower frequencies comes mainly from the periphery of the loop, where the plasma density is much lower than at the axes and Razin suppression is almost negligible. As we can see from Figure 18, the overall spectrum has a much flatter low frequency slope (solid line) than the corresponding spectrum from a homogeneous source (dashed line). Taking into account the fact that in cylindrical geometry the source at lower frequencies becomes larger we get a even flatter spectrum (dotted line). From the spectral shape alone, one cannot distinguish these inhomogeneous spectra from an ordinary GS-spectrum (one without Razin suppression).

References

Bai, T.: 1986, *Astrophys. J.* **308**, 912.
Bastian, T. S., Benz, A. O, and Gary, D. E.: 1998, *Ann. Rev. Astron. Astrophys.* **36**, 131.
Bastian, T.S.: 2006, In: *Solar Physics with the Nobeyama Radioheliograph, Nobeyama Solar Radio Observatory Report* **1**, 3.
Bastian, T. S., Fleishman, G. D., Gary, D. E.: 2007, *Astrophys. J.* **666**, 1256.
Belkora, L.: 1997, *Astrophys. J.* **481**, 532.
Dulk, G. A., Marsh, K. A.: 1982, *Astrophys. J.* **259**, 350.
Dulk, G. A., Kiplinger, A. L., Winglee, R. M.: 1992, *Astrophys. J.* **389**, 756.
Fleishman, G. D., Melnikov, V. F.: 2003, *Astrophys. J.* **587**, 823.
Fleishman, G. D., Nita, G. M., Gary, D. E.: 2005, *Astrophys. J.* **620**, 506.
Gary, D. E., and Hurford, G. J.: 2000, In: Bastian, T. S., Gopalswamy N., Shibasaki K. (eds.), *Solar Physics with Radio Observations, NRO Report* **479**, 429.
Gary, D. E.: 1985, *Astrophys. J.* **297**, 799.
Gary, D. E., Hurford, G. J.: 2004, In: Gary, D. E., Keller, C. U. (eds.), *Solar and Space Weather Radiophysics*, Springer, 69.

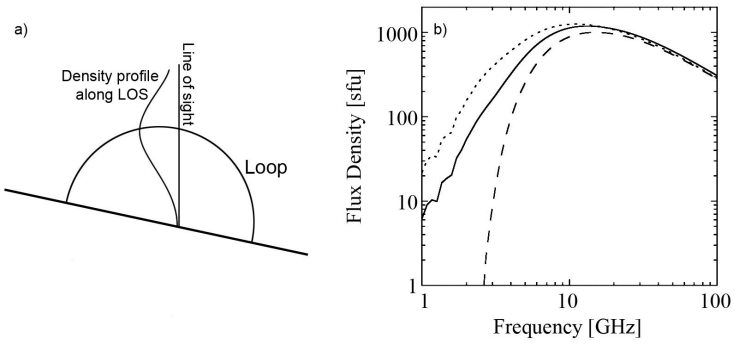

Figure 18. Influence of a plasma density inhomogeneity on the low frequency slope of the gyrosynchrotron spectrum. (a) Sketch of the model geometry used. The gaussian curve shows the profile of both ambient and energetic electron density along the line of sight (see text for details). (b) Dashed line: The classical Razin suppressed spectrum as it would appear for a homogeneous source with the parameters on the loop axis. Solid line: The spectrum obtained along the line of sight in (a), due to the inhomogeneity in the model. Dotted line: The spectrum obtained with the same conditions as for the solid line spectrum, but with weighting to account for the radial dependence of area in a cylindrical geometry.

Ginzburg, V.L.: 1953, *Uspekhi Fiz. Nauk* **51**, 343.
Guidice, D. A., Castelli, J. P.: 1975, *Solar Phys.* **44**, 155.
Klein, K.-L.: 1987, *Astron. Astrophys.* **183**, 341.
Klein K.-L., Trottet G.: 1984, *Astron. Astrophys.* **141**, 67.
Klein, K.-L., Trottet, G., Magun, A.: 1986, *Solar Phys.* **104**, 243.
Krucker, S., Hurford, G. J., MacKinnon, A. L., Shih, A. Y., Lin, R. P.: 2008, *Astrophys. J.* **678**, 63.
Lee, J. W.: 2004, In: Gary, D. E., Keller, C. U. (eds.), *Solar and Space Weather Radiophysics*, Springer, 177.
Lee, J. W., Gary, D. E.: 2000, *Astrophys. J.* **543**, 457.
Melnikov, V. F., Silva, A. V. R.: 2000, In: Ramaty, R., Mandzhavidze, N. (eds.), *High Energy Solar Physics Workshop — Anticipating Hessi*, *ASP Conf. Ser.* **206**, 475.
Melnikov, V. F., Shibasaki, K., Reznikova, V. E.: 2002, *Astrophys. J.* **580**, L185.
Melnikov, V.F., Reznikova, V.E., Shibasaki, K., Nakariakov, V.M.: 2005, *Astron. Astrophys.* **439**, 727.
Nita, G. M., Gary, D. E., Lee, J.W.: 2004, *Astrophys. J.* **605**, 528.
Petrosian, V.: 1981, *Astrophys. J.* **251**, 727.
Preka-Papadema, P., Alissandrakis, C. E.: 1988, *Astron. Astrophys.* **191**, 365.
Ramaty, R.: 1969, *Astron. J.* **158**, 753.
Ramaty, R., Schwarz, R.A., Enome, S., Nakajima, H.: 1994, *Astrophys. J.* **436**, 941.
Razin, V.A.: 1960a, *Izv. Vyssh. Uchebn. Zaved. Radiofiz.* **3**, 584.
Razin, V.A.: 1960b, *Izv. Vyssh. Uchebn. Zaved. Radiofiz.* **3**, 921.
Silva, A. V. R., Wang, H., Gary, D. E.: 2000, *Astrophys. J.* **545**, 1116.
Simões, P. J. A., Costa, J. E. R.: 2006, *Astron. Astrophys.* **453**, 729.
Stähli, M., Gary, D. E., Hurford, G. J.: 1989, *Solar Phys.* **120**, 351.
Takakura, T., Kai, K.: 1961, *Publ. Astron. Soc. Japan* **13**, 94.
Takakura, T., Kai, K.: 1966, *Publ. Astron. Soc. Japan* **18**, 57.
Takakura, T.: 1972, *Solar Phys.* **26**, 151.
Twiss, R.Q.: 1954, *Philos. Mag.* **45**, 249.
Wiehl, H., Batchelor, D. A., Crannel, C. J., Dennis, B. R., Price, P. N., Magun, A.: 1985, *Solar Phys.* **96**, 339.